International Journal of Climatology

International Journal of Climatology | RMetS

RESEARCH ARTICLE OPEN ACCESS

Atmospheric Pressure Rivalry Between the Arctic and Northern Pacific: Implications for Alaskan Climate Variability

Igor V. Polyakov[1] | Thomas J. Ballinger[2] | James E. Overland[3] | Stephen J. Vavrus[4] | Seth L. Danielson[5] | Rick Lader[2] | Uma S. Bhatt[6,7] | Amy S. Hendricks[6] | Franz J. Mueter[5]

[1]International Arctic Research Center and College of Natural Science and Mathematics, University of Alaska Fairbanks, Fairbanks, Alaska, USA | [2]International Arctic Research Center, University of Alaska Fairbanks, Fairbanks, Alaska, USA | [3]NOAA Pacific Marine Environmental Laboratory, Seattle, Washington, USA | [4]Nelson Institute Center for Climatic Research, University of Wisconsin – Madison, Madison, Wisconsin, USA | [5]College of Fisheries and Ocean Sciences, University of Alaska Fairbanks, Fairbanks, Alaska, USA | [6]Department of Atmospheric Sciences, University of Alaska Fairbanks, Fairbanks, Alaska, USA | [7]Geophysical Institute, University of Alaska Fairbanks, Fairbanks, Alaska, USA

Correspondence: Igor V. Polyakov (ivpolyakov@alaska.edu)

Received: 13 June 2024 | **Revised:** 23 August 2024 | **Accepted:** 16 September 2024

Funding: This research was supported by Office of Naval Research (N00014-21-1-2577), National Science Foundation (1724523, 2053084, 2043727), NOAA Global Ocean Monitoring and Observing (GOMO) (5612), and National Aeronautics and Space Administration's Arctic Boreal Vulnerability Experiment (80NSSC22K1257).

Keywords: climate change | Pacific Arctic | sea level pressure patterns

ABSTRACT

Located at the confluence of the Arctic and North Pacific and with Alaska at its heart, the Pacific Arctic Region (PAR) is a unique and interconnected regional climate system. Significant climatic changes in the PAR are described by a novel, mobile monthly Alaska Arctic Front (AAF) index, which is defined by sea level pressure differences between the migratory cores of the Beaufort High and Aleutian Low. Regional climate variability associated with the AAF shows prominent decadal signatures that are driven by the opposing effects of the North Pacific and the Arctic atmospheric pressure fields. Low AAF (negative phase) is dominated by North Pacific forcing, whereas high AAF (positive phase) is dominated by Arctic atmospheric processes. The recent (2011–2021) negative AAF phase, which is associated with the westward displacement of Aleutian Low explaining stronger northward winds and enhanced water transport northward through Bering Strait, is conducive to increased oceanic heat and freshwater content, reduced regional sea ice cover in the PAR, and to the expansion of Pacific species into the Arctic. These factors are all indicators of the Pacification of the Arctic Ocean, a key feature of climate change related to progression of anomalous Pacific water masses and biota into the polar basins. It is not yet clear if or when the recent phase of decadal variability will change and alter the rate of Pacification of the Arctic climate system.

1 | Introduction

Arctic sea ice loss and atmospheric warming have increased significantly in recent decades, and both trends have emerged as primary indicators of global warming, suggesting that the Arctic is undergoing notable and possibly irreversible changes (Box et al. 2019). Pan-Arctic climate variability and changes, however, are not uniform in time, and are modulated by the interannual to decadal-scale atmospheric forcings such as the Arctic Oscillation (AO) and Arctic Dipole (AD) (e.g., Overland et al. 2012; Proshutinsky et al. 2015). When the AD is positive, as it has been during the recent decade, anticyclonic surface pressure and winds prevail over North America and cyclonic winds occur over Eurasia on climate timescales (Overland and

Wang 2005; Polyakov et al. 2023). The current positive AD phase (AD+) began in 2007 and has directly impacted the Arctic climate and cryosphere. It has weakened northward oceanic inflows and enhanced sea ice export across Fram Strait, increased inflows throughout the Barents Sea, and favoured stronger Arctic Ocean circulation. The AD+ phase also contributed to slowing sea ice loss in the Amerasian Basin (Figure S1; for this and other geographical names, see Figure 1) by moving freshwater from the Siberian shelves, increasing regional stratification, and lowering vertical oceanic heat fluxes after 2007 (Polyakov et al. 2023).

Regional climatic changes may, however, follow distinct patterns. For example, the Pacific Arctic Region (PAR), loosely bounded by the Bering Sea on the south and the Amerasian Basin with its adjoining shelves on the north, is a unique and interconnected regional system. Encompassing the confluence of the Arctic and Pacific, the physical, biological, and socio-ecological components of the system are exhibiting rapid changes (Huntington et al. 2020). As we will show further, the origins of PAR variability are different from those controlling pan-Arctic variability in recent decades, which has been dominated by the AD. Furthermore, given the complex origins of regional climate variability, there is evidence that using a single climate index to explain climate anomalies may be an oversimplification (McAfee 2016). For instance, the Pacific Decadal Oscillation (PDO) index shows significant variations in the amplitude of circulation patterns, surface temperature, and precipitation anomalies of the North American winters between comparable PDO phases (McAfee 2014). Following this background, in this study we examine how the Pacific Arctic sector relates to co-variations in atmospheric patterns in the North Pacific and Arctic (the Aleutian Low [AL] and Beaufort Sea High). We will demonstrate that the importance of factors controlling the PAR climate changes in time.

Many of the observed PAR changes have been associated with anomalous sea ice loss (e.g., Ballinger and Overland 2022). The rates of sea ice decline were strong both in the Amerasian Basin in summer (up to $1.5\times10^4\,km^2$/year prior to 2007; see figure 1e in Polyakov et al. 2023) and over the Bering Sea shelf in winter (Thoman et al. 2020). However, in response to the redistribution of freshwater from the Siberian shelves into the Amerasian Basin caused by anomalous winds and increased stratification that suppresses vertical oceanic heat fluxes, the regional sea ice area in the basin actually increased since 2007, remaining about 5%–35% below the 30-year mean (Polyakov et al. 2023). Meanwhile, the annual mean sea ice concentration (SIC) trend in the Bering Sea contrasts with that of the Arctic (Frey et al. 2025); over 1980–2021 the Bering ice trend was positive, $0.70\pm0.29\%$ per decade, with 2012 exhibiting record high and 2018 experiencing record low sea ice coverage. Ice conditions are governed largely by the regional wind field and upper ocean heat content (Thoman et al. 2020; Wang, Jing, and Guo 2024) (Figure S1). Extreme Bering Sea ice loss occurred during consecutive winters of 2017–2018 and 2018–2019 (Stabeno and Bell 2019; Overland et al. 2024), which altered the timing of subsistence activities by coastal Alaska Native hunters (Hauser et al. 2021) and triggered northward displacements of commercially important fish stocks, in particular walleye pollock (*Gadus theragrammus*), Pacific cod (*Gadus macrocephalus*) and several flatfish species (Stevenson and Lauth 2019). Warm waters associated with the region's ice loss appear to have caused the collapse of the economically important eastern Bering Sea snow crab (Szuwalski et al. 2023).

The recent decades were also marked by strong climatic changes in Alaska's continental shelf waters and the adjoining basins. The eastern Bering Sea shelf experienced statistically significant warming of surface waters and freshening of the water column over the length of the instrumental records which started in the mid-1960s (Danielson, Akhinga et al. 2020, their figure 7). The processes accelerated in the 2010s, promoting enhanced air-ocean heat exchanges and advection of oceanic heat northward through Bering Strait into the Arctic, with the additional loss of Arctic sea ice, freshening of the upper ocean, and the northward spread of biota (Danielson, Ahkinga et al. 2020; Timmermans

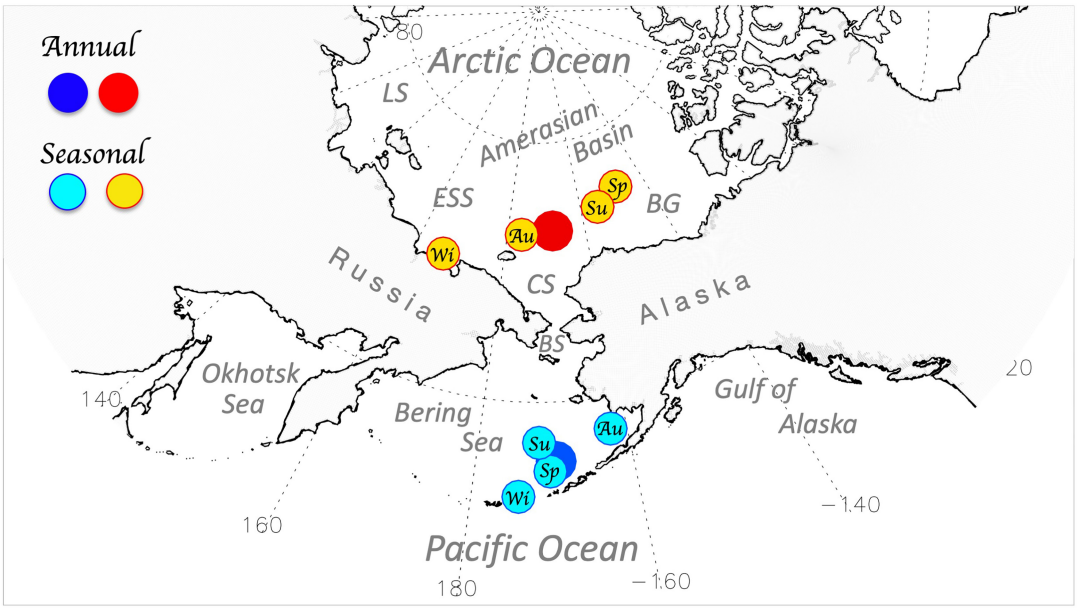

FIGURE 1 | Pacific Arctic Region (PAR) and annual and seasonal mean positions from 1959 to 2021 of the Beaufort High (BH, red/yellow) and Aleutian Low (AL, blue). LS, ESS, CS, BG, and BS indicate Laptev Sea, East Siberian Sea, Chukchi Sea, Beaufort Gyre, and Bering Strait, respectively.

and O'Toole 2023; Baker et al. 2023). On the Chukchi shelf, the warming rate since 1990 tripled, capping a century-long warming of 1.4°C that was not accompanied by significant changes in salinity (Danielson, Ahkinga et al. 2020). Anomalous oceanic heat transport across the Bering/Chukchi shelves is received by the Amerasian Basin, where they impact the heat and freshwater content in the Arctic's halocline (e.g., Steele et al. 2004; Timmermans et al. 2014; Timmermans, Toole, and Krishfield 2018; Polyakov et al. 2020; Woodgate and Peralta-Ferriz 2021) and affect the northward expansion of Pacific species' distributions into the Arctic (Ershova et al. 2015; Baker et al. 2023).

PAR sea ice decline and warming across the ocean–atmosphere interface amplify turbulent heat exchange between the ocean and the atmosphere, affecting the region's weather variability at short and long-term scales. For example, stronger heat transfer from the upper ocean to the atmosphere can modify the local atmospheric pressure field. This process provides additional energy to intermittent, overlying high-pressure ridges within the polar jet stream (Ballinger and Overland 2022) as was the case documented by Tachibana et al. (2019) for the winter of 2017–18. Turbulent heat transfer is also associated with decreasing static stability and increasing horizontal wind shear, which are linked with intensification of wintertime cyclones travelling from the Bering Sea northward into the Arctic Ocean since 1979 (Crawford et al. 2022).

Increased variability of the position and strength of the Beaufort High (BH), typically centred over the Canada Basin and associated with anticyclonic winds, played a critical role in these changes. For instance, during considerable portions of the winters in 2017 and 2020, the BH and associated Beaufort Gyre—a prominent component of the Arctic sea ice and upper ocean circulation—unexpectedly vanished (Moore et al. 2018; Ballinger et al. 2021). The winter of 2020/21 was also highly unusual, and featured an extraordinarily strong BH and the second-highest winter sea-level pressure (SLP) north of 60° N since 1979 that resulted in significant sea ice redistributions in the central Arctic (Mallett et al. 2021).

The 2017–2021 period was also notable for environmental changes south and west of Alaska (Ballinger and Overland 2022). The wintertime AL, a primary determinant of climate variability in the Bering Sea (e.g., Rodionov, Overland, and Bond 2005) that is typically extended west-to-east along the Aleutian Island chain, was shifted well to the west. The location of the SLP pattern promoted persistent southerly wind events and helped much of the south-central Bering Sea avoid freeze-up during the winters of 2017–18 and 2018–19 (Stabeno and Bell 2019; Ballinger and Overland 2022). The distribution of these anomalous ice-free areas and southern ice edge positions exceeded even 2030–2044 projections from phase 5 of the Coupled Model Intercomparison Project (Wang et al. 2018).

Distinct temperature and SLP characteristics between areas in which the AL and BH migrate help to sustain an atmospheric Arctic frontal zone through much of the year (Serreze, Lynch, and Clark 2001; Overland, Wang, and Ballinger 2018). However, despite their role in shaping PAR long-term variability and recent climatic changes, the AL and BH semi-permanent SLP features are often studied in isolation (e.g., Rodionov, Overland, and Bond 2005; Mallett et al. 2021; Ballinger et al. 2021). Recently, Cox et al. (2019) introduced a climate index including their interaction based on 850-hPa geopotential height at four fixed grid-point locations (three south and one north of Bering Strait). The authors showed that this index is correlated with the melting of snow in northern Alaska and the onset of sea ice melt in adjacent waters. Similarly, Danielson et al. (2014) used four grid point locations (two north and two south of Bering Strait) to assess the relative strengths and locations of the BH and the AL, relating the atmospheric structure to underlying oceanic responses in the basins and on the continental shelves. However, the non-stationary nature of the seasonal AL and BH patterns (see, e.g., the monthly BH and AL positions for 1959–2021 in Figure 2) plays a key role in shaping the synoptic-scale gradient wind regime, which, depending on whether it is meridional or zonal, either connects or isolates the sub-Arctic to Arctic interaction.

The aforementioned past research motivated development of the Alaska Arctic Front (AAF) index, which is designed to account for the migratory nature of the AL and BH co-variability in shaping PAR climate. It is designed in a manner akin to the Portis et al. (2001) mobile North Atlantic Oscillation (NAO) Index, which traces the Icelandic Low and Azores High pressure cells in a spatiotemporal context. More recently, Moore, Renfrew, and Pickart (2013) discussed the multidecadal mobility of the NAO's centres of action. The analysis presented by Franzke and Feldstein (2005) demonstrated that the NAO is the teleconnection pattern driven almost entirely by transient eddy vorticity fluxes. In this work, our primary aims are to describe the geographic and temporal characteristics of the AAF from 1959 to 2021, evaluate its impacts on regional near-surface meteorological and oceanographic conditions, and compare and contrast the index with other modes of climate variability that influence the PAR. We also demonstrate some examples of regional multidisciplinary applications of the AAF index that may be expanded upon in future research.

2 | Data and Methods

2.1 | Atmospheric Data From ERA5 Reanalysis

Monthly surface air temperatures (SAT), SLP, and 10 m winds during 1959–2021 used in this study are from the European Centre for Medium-Range Weather Forecasts reanalysis ERA5 (Hersbach et al. 2020), downloaded from https://cds.climate.copernicus.eu/cdsapp#!/home. The horizontal resolution of the data is 0.25°. Despite the ERA5 data record extending from 1940 to present, our analyses herein commenced with its early data release from 1959 onward. This starting follows the International Geophysical Year of 1957–1958 when atmospheric reanalyses are more reliable in the high latitudes, including Alaska, due to an increased number of assimilated surface observations and standardisation of radiosonde launch times (Grant et al. 2009; Walsh et al. 2018; Ballinger et al. 2023). The quality of atmospheric reanalysis products was greatly improved in the post 1979 period when the satellite data became available.

2.2 | Bering Strait Mooring Data

Moored data from the Bering Strait provides direct measures of heat, freshwater and volume fluxes from the North Pacific into the Arctic (Woodgate 2018). The Bering Strait mooring period of

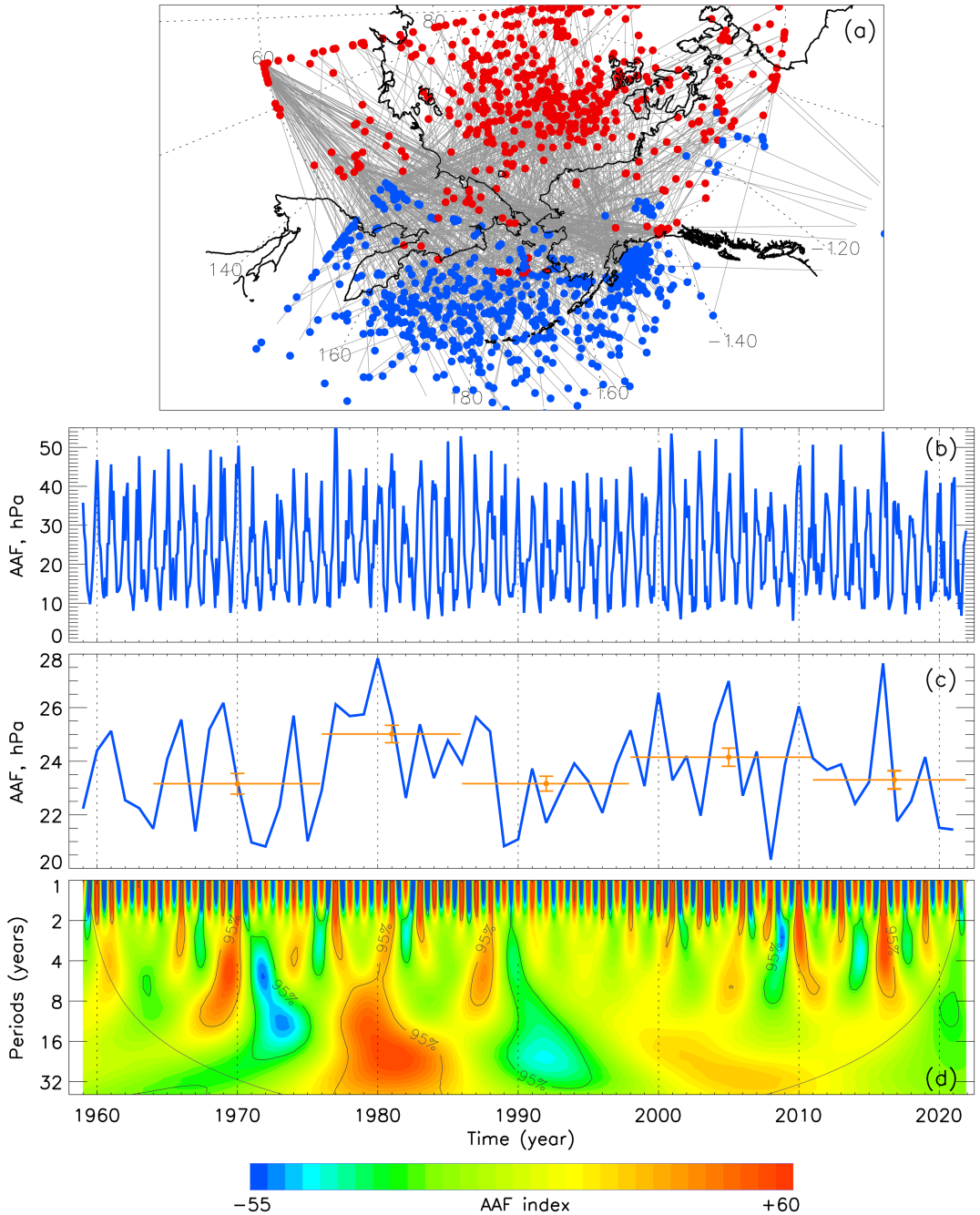

FIGURE 2 | (a) The monthly sea level pressure (SLP) difference between the Beaufort High (BH, red dots) and the Aleutian Low (AL, blue dots) is what is referred to as the mobile Alaska Arctic Front (AAF) index. Grey lines connect monthly BH and AL pairs used to create the AAF index for the 1959–2021 period. (b) The AAF monthly time series (note the significant seasonal cycle and decadal mode of variability in the AAF time series), (c) the annual AAF index with multiyear means (red; standard errors are shown by segments) and (d) the mobile AAF index's wavelet (grey lines identify areas with 95% confidence level and black lines show cones of influence).

record begins in 1990 and continues through 2021, with a gap in the mid-1990s. Monthly water transports (Sv, $1\text{Sv} = 10^6\,\text{m}^3/\text{s}$) are used in this study. Data are available at https://psc.apl.washington.edu/HLD/Bstrait/Data/BeringStraitMooringDataArchive.html.

2.3 | Climatological Indices

Monthly climate indices (they are available in https://www.psl.noaa.gov/data/climateindices/list/) broadly associated with PAR atmospheric variability (e.g., Papineau 2001; Duffy et al. 2005; Rodionov, Overland, and Bond 2005; Ballinger and Rogers 2014; Bhatt et al. 2021) are examined against the AAF index. These include the AD, AO, East Pacific/North Pacific (EP/NP) Oscillation, Niño 4 index, North Pacific Index (NPI), PDO, Pacific North American (PNA) index, and the Southern Oscillation Index (SOI). The AD is defined as the second leading mode of the Empirical Orthogonal Function analysis of the monthly SLP. The other monthly climate indices are obtained from and defined within NOAA's Physical Sciences Laboratory (PSL) archive.

2.4 | Terrestrial Data

The time-integrated Normalized Difference Vegetation Index (TI-NDVI), a remotely sensed proxy for Arctic vegetation productivity used in this study is from the GIMMS NDVI3g V1.2 product (Pinzon and Tucker 2014). Time series for TI-NDVI is averaged over the Yukon-Kuskokwim Delta region (YKD), bounded by the Yukon Delta National Wildlife Refuge and the YKD ecoregion (Frost et al. 2021; Nowacki et al. 2003) for pixels below 300 m, used previously to investigate climate drivers of tundra trends (Frost et al. 2021; Hendricks et al. 2023). GIMMs3g NDVI data are available from the NASA ABoVE Oak Ridge National Laboratory (Pinzon et al. 2023) Distributed Active Archive Center available at https://daac.ornl.gov/.

2.5 | Sea Ice Concentration

Global daily SIC is from 1981 to 2021 with 0.25×0.25° spatial resolution (https://psl.noaa.gov/data/gridded/data.noaa.oisst.v2.highres.html, Huang et al. 2021). In addition to pan-Arctic data, spring sea ice was investigated using the Special Sensor Microwave Imager SIC data from 1982 to 2019 (Comiso and Nishio 2008). Spring SIC is the percentage of a pixel covered by ice during early spring (averaged from 16 April to 6 May, a 3-week period when the sea ice is climatologically 50% concentration) for the eastern part of the Bering sea (along coastal Alaska) was used in this study.

2.6 | Biological Indices

In our analyses, we examined two biological indices. To capture trends in the spatial distribution of the fish community, we used a measure of the average North–South displacement of major fish and invertebrate taxa from their respective centres of gravity. This measure was based on summer bottom trawl surveys conducted by NOAA Fisheries every summer from 1982 to 2022 (https://www.fisheries.noaa.gov/alaska/science-data/groundfish-assessment-program-bottom-trawl-surveys). We will refer to this index as F1. No data were available for 2020 due to the lack of a survey that year (we used linear interpolation to close this gap). The index is based on the catch per unit effort (CPUE, kg/ha) of 46 taxa described in Mueter and Litzow (2008). Annual latitudinal centres of gravity for each taxon were computed as the CPUE-weighted mean latitude across 343 standard survey stations that were sampled consistently across the time series. Each station was further weighted by the approximate area that it represents. Species-specific mean annual latitudes were centred on zero by subtracting the long-term mean latitude and the annual north–south displacement from the long-term mean position for each taxon (in km) were computed. Finally, species-specific annual north–south displacements were averaged across taxa to obtain an overall average displacement.

The second (F2) index used in this study provides a measure of the overall biomass of benthic fish and invertebrates on the eastern Bering Sea shelf. The index is based on the catch-per-unit-effort (CPUE in kg/ha) of each species or taxon at each successful haul completed during standardised bottom trawl surveys from 1982 to 2022. Total CPUE for each haul was computed as the sum of the CPUEs over all fish and invertebrate taxa. To account for gaps in spatial coverage and variable survey timing we modelled log-transformed total CPUE ($N = 14{,}842$ hauls) as a smooth function of Julian Day and location (latitude/longitude) using a Generalised Additive Model. Year-specific intercepts from the model (1982–2022), corresponding to log(CPUE) at the median latitude, longitude and sampling day, were used as the final index.

2.7 | Defining and Analysing the AAF Index

Monthly ERA5 SLP gridded data were used to construct the mobile AAF index (Figure 2). The position of the BH was defined as the maximum SLP within the domain limited by 65°–85° N and 120°–270° E. Similarly, the position of the AL was defined as a minimum SLP within the domain limited by 45°–60° N and 160°–240° E. These domains were selected following the BH and AL spatial variability noted by Serreze and Barrett (2011) and Rodionov, Overland, and Bond (2005). The AAF index is defined as the corresponding monthly difference between the BH and AL extremes (i.e., BH minus AL). Seasonal values are averaged from monthly data as follows: winter (DJF), spring (MAM), summer (JJA), and autumn (SON). Annual AAF time series are averaged from monthly means within the calendar year. Sensitivity experiments with changes of the domain boundaries showed robustness of our definition (Figure S2).

Wavelet analysis was used to define the amplitudes and phases of variability for different periods in various time series. For example, wavelet analysis applied to the AAF time series isolated three distinct temporal signatures of AAF decadal variability since the mid-1980s. We then composite PAR SAT, SLP, and SIC fields for each period to gain insight into how AAF phasing influences the regional surface climate (see Section 3.3). The package of wavelet programs is used for the calculation of wavelet transforms based on the DOG Mother function (Torrence and Compo 1998). The 95% confidence intervals and cones of influence shown in wavelet presentations are provided by the same package. All of the time series were linearly de-trended before the wavelet analysis was applied.

Trends in the time series were evaluated by the least squares best-fit method. Their statistical significance is estimated using Student's t statistics following Brooks and Carruthers (1953) taking into account that the degree of freedom depends on the red noise (internal correlation). For a time series of red noise, it has been suggested that the degree of freedom DOF can be determined as $\mathrm{DOF} = N\Delta t/2T_e$ where N is the length of time series, Δt is the time step, and T_e is the e-folding decay time of autocorrelation (Panofsky and Brier 1958). Statistical significance of cross-correlations used in the analyses also takes into account internal correlation; however, due to high decorrelation, this had little effect on the significances of the cross-correlations.

3 | Results

3.1 | Modes of Variability

The monthly mobile AAF index time series and its wavelet transform are shown in Figure 2 for the full period of analysis. Strong seasonality dominates the record, as evidenced by

the peak power concentrated throughout the wavelet's annual cycle (Figure 2b). Another statistically significant mode of variability is found at the decadal scale, which exhibits maximum energy at periods of roughly 10–15 years. We will show in following sections that this decadal mode of the AAF variability is clearly expressed in Alaskan marine, sea ice, and terrestrial records. Over the course of the record (1959–2021), the annual and seasonal AAF time series do not show statistically significant trends; however, they do show strong decadal variability with positive and negative phases lasting 10–15 years; the pattern is influenced at 4- to 10-year periods in spring, winter, and autumn by noise from shorter-term interannual variability (Figure 3).

3.2 | Drivers of Variability

Assessing correlations of the annual and seasonal AAF time series against key indices of climate variability allows identification of the Alaskan regional processes with variability at broader geographical scales. The surprising lack of correlation between the AAF index and the AD index (Figure 4) is in contrast with

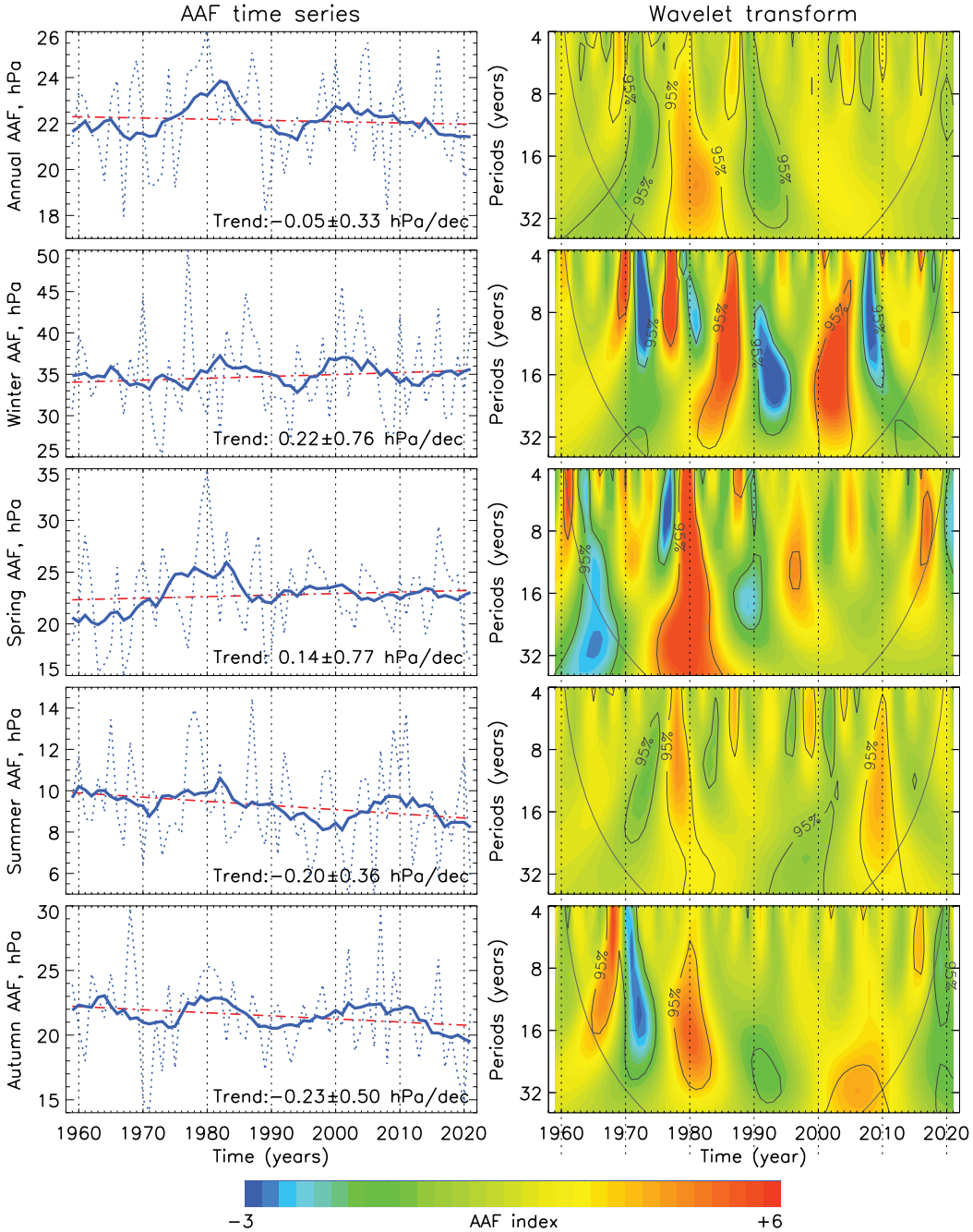

FIGURE 3 | Time series (left) and wavelets (right) of the annual and seasonal mobile AAF index. Annual and seasonal time series are shown by dotted lines, 7-year running mean time series are shown by solid lines. Red broken lines show linear trends (also shown in the bottom right of each panel). In wavelet panels, grey lines identify areas with 95% confidence level and black lines show cones of influence.

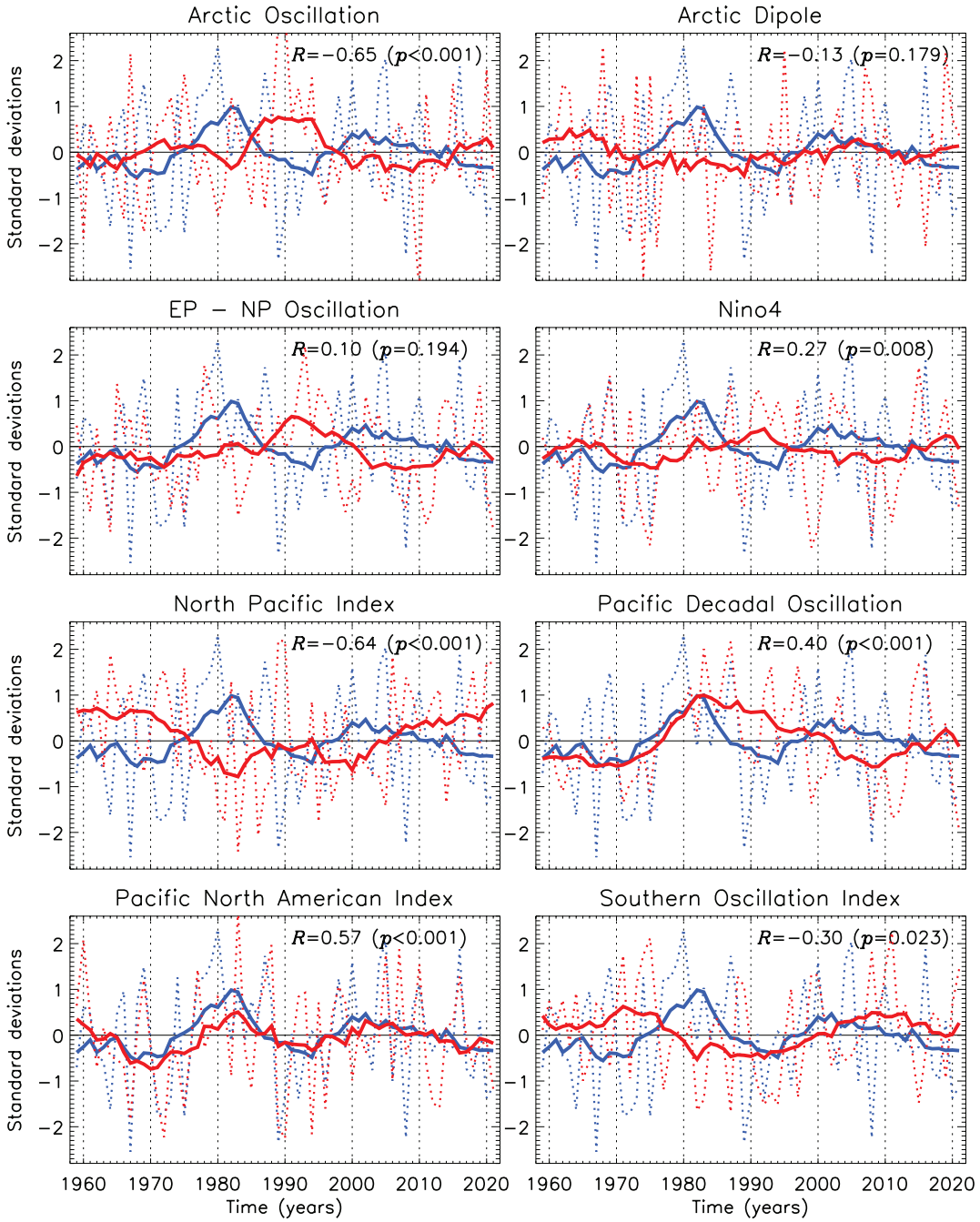

FIGURE 4 | Time series of the *annual* AAF index (blue time series) and other important climate indices (red time series) for 1959–2021 (all detrended). Annual time series are shown by dotted lines, 7 years running mean time series are shown by solid lines. The time series are reduced to their anomalies by subtracting their 1991–2020 means and normalised by their respective standard deviations. Correlation (R) based on unsmoothed data is significant at the 95% confidence level for $p < 0.05$.

the results of a pan-Arctic synthesis (Polyakov et al. 2023) and raises the possibility that other causes could be responsible for the variations observed in Alaska's regional climate. Indeed, the mobile AAF and three indices—two Pacific (NPI and PNA) and one Arctic (AO)—are reasonably well correlated, as shown in Figure 4 (estimates of correlation, R, based on unsmoothed data are given in each panel). In the analysis that follows the PNA is used as an indicator of PAR climate changes driven by the North Pacific, and we note a strong cross-correlation ($R = -0.86$) between the NPI and PNA. The AO will be used as an indicator of Arctic changes impacting PAR climate. Note that statistically significant correlations between the AAF and both the AO and PNA are found for each of the four seasons (Figure 5).

It is worthwhile to look further into the factors controlling regional PAR climate variability. For 1959–2021, we found stronger correlation of the BH SLP with the AO index and weaker correlations with the PNA; the opposite is true for the AL (Figures S3 and S4). However, one-point correlation maps of the ERA5 SLP with AAF, AO, NPI and PNA indices suggest that the AAF is strongly modulated by the two regional patterns—the AO and the PNA (Figure 6). The AAF and SLP correlation

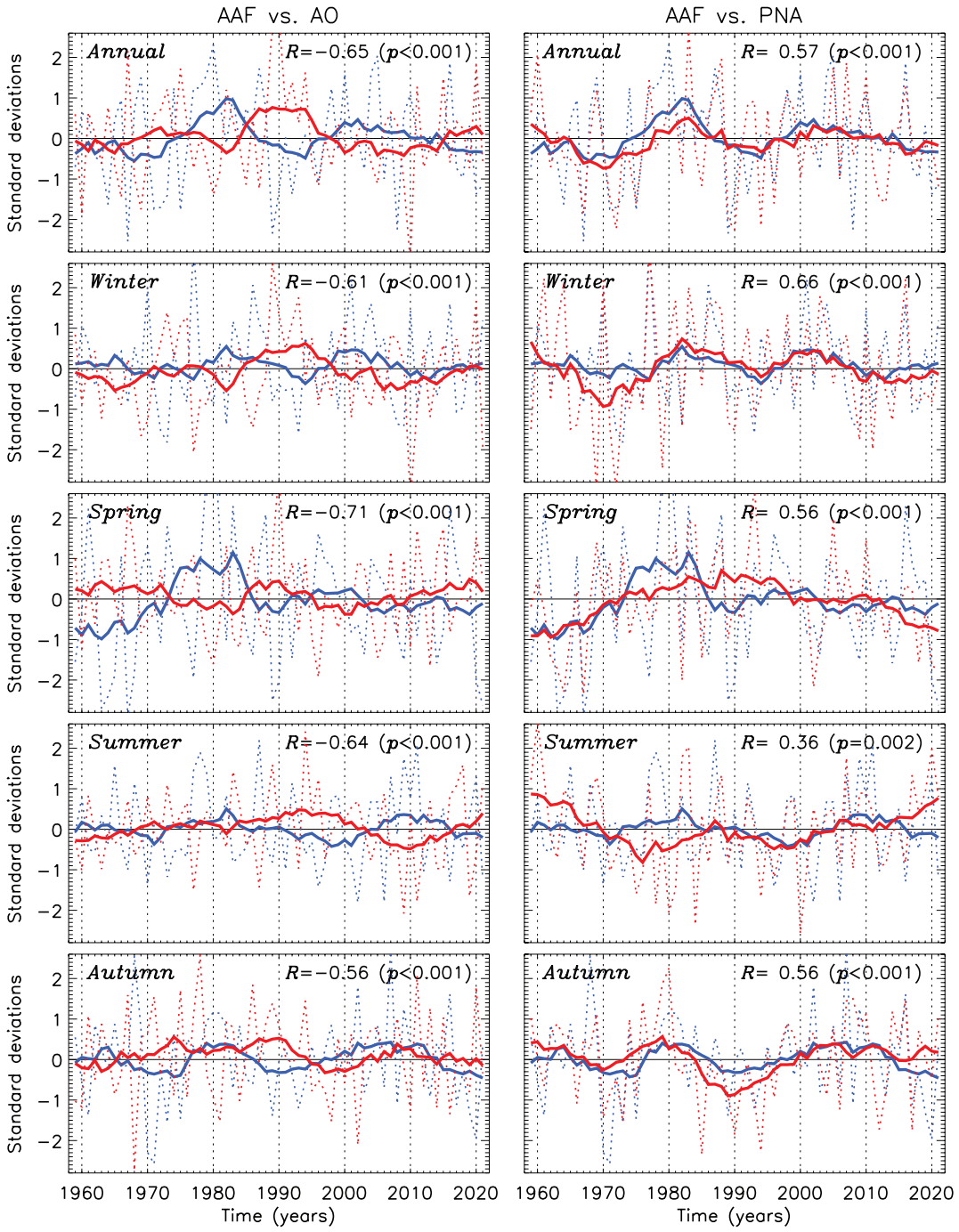

FIGURE 5 | Correlation (*R*) between the annual and seasonal AAF index (blue time series) and Arctic Oscillation (AO, left) and Pacific North American (PNA, right) indices (red time series) for 1959–2021 (all detrended). The time series are reduced to their anomalies by subtracting their 1991–2020 means and normalised by standard deviations. Annual time series are shown by dotted lines, 7 years running mean time series are shown by solid lines. *R* based on unsmoothed data is significant at the 95% confidence level for $p < 0.05$.

exhibit a dipole-like pattern, with a stronger (positive) correlation in the Arctic similar to the AO index and a stronger (negative) correlation in the Pacific sector of the PAR region similar to the PNA. Surface air temperature (SAT) over the Canadian Arctic Archipelago shows a strong positive correlation with the AAF, while over the southwestern Bering Sea the correlation is negative; this pattern is linked to the PNA and NPI. The correlation pattern between SIC and AAF is intricate, with a notable characteristic being the highest correlation observed in the East Siberian Sea, which is also evident in the AO and SIC correlation patterns.

3.3 | Composites of Decadal Variability

Next, we use the AAF index, a measure of the regional climate variability in the PAR, to examine the differences between ~10–15-year phases of the decadal mode of variability. This study

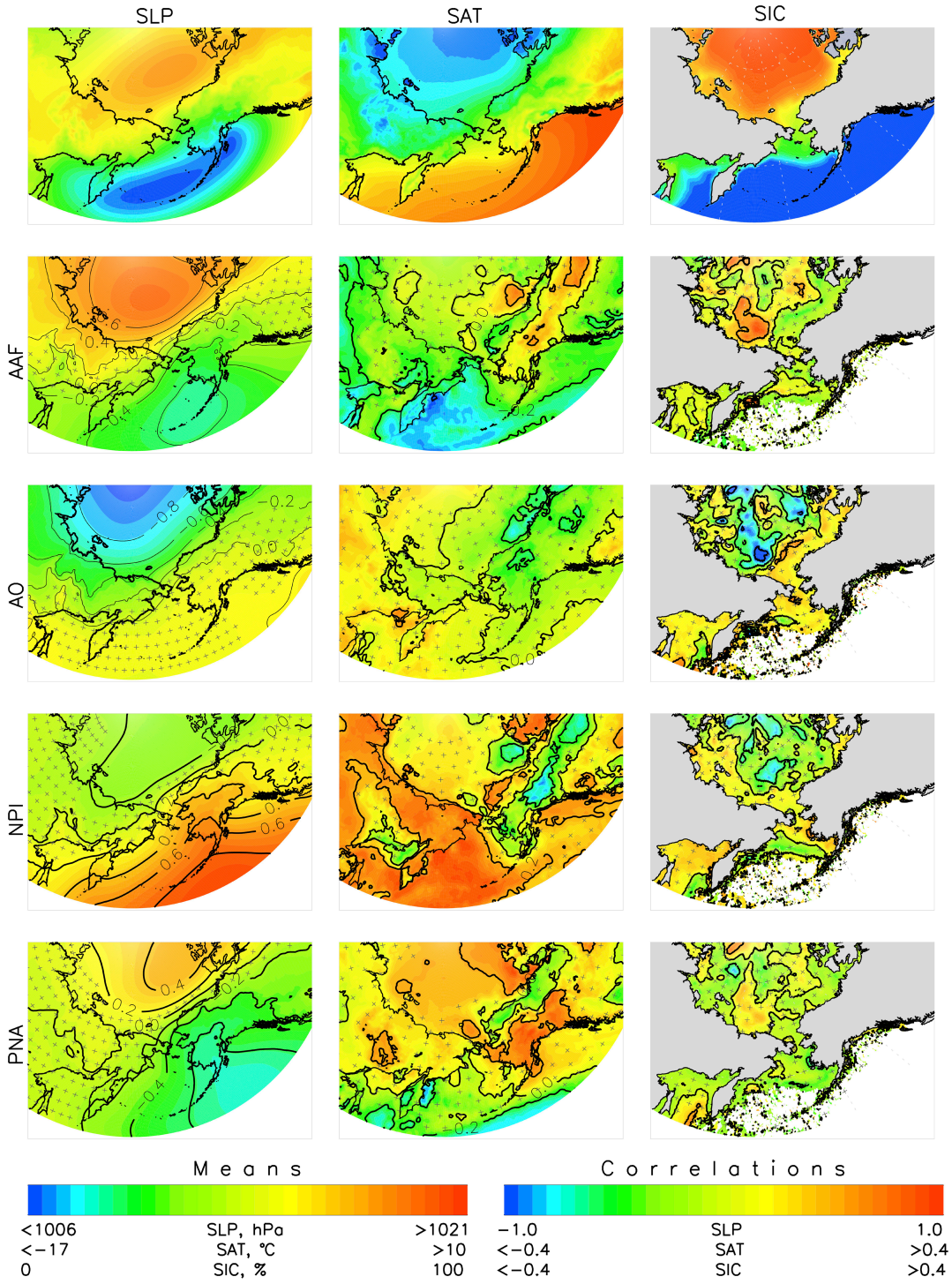

FIGURE 6 | Maps of annual mean 1986–2021 SLP, SAT, and SIC (top) and their correlations with the AAF, AO, NPI, and PNA indices (bottom four rows). Stippling is used to mark areas where correlations are not statistically significant at 95% confidence level.

explores the three most recent phases: a positive phase from 1998 to 2010 and two negative phases from 1986 to 1997 and 2011 to 2021 (Figure 2).

The positive AAF phase dominated in 1998–2010 and was associated with an enhanced BH and AL and stronger anticyclonic winds throughout the central Arctic and cyclonic winds in the eastern Bering Sea and over the Gulf of Alaska (Figure 7). Extremely cold weather was prevalent in the northwest Bering Sea, with relatively low temperatures over mainland Alaska, Siberia and the North Pacific. Local increases in sea ice area were associated with anomalous (relative to the 1986–2021 means) southward winds across the northern Bering Sea and westward winds over the Siberian shelf seas, while sea ice area declined in the Beaufort

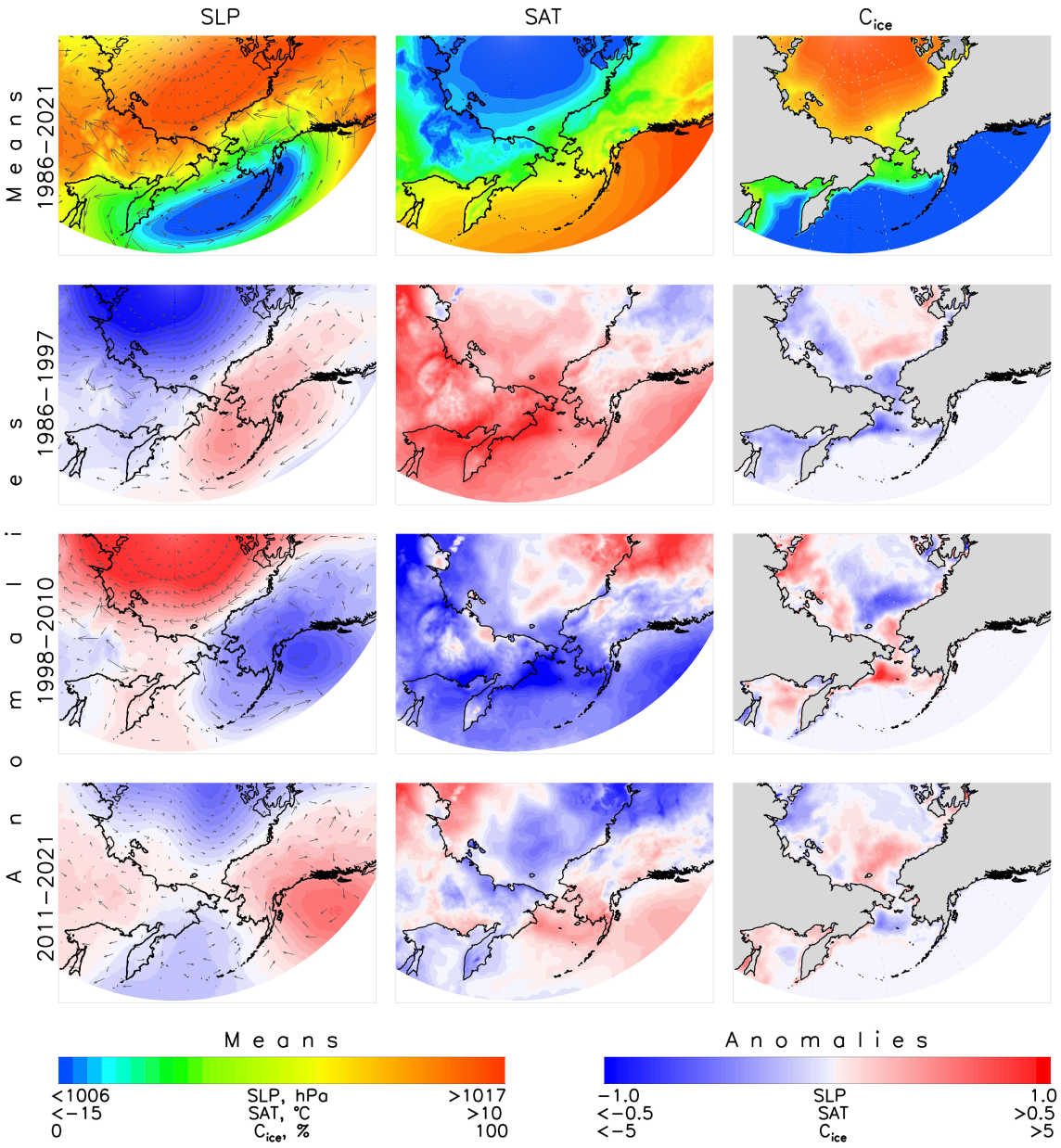

FIGURE 7 | (Top row) Annual mean 1986–2021 sea level pressure (SLP, colour) and geostrophic wind (vectors, left), surface air temperature (SAT, middle), and sea ice concentration (SIC, right) and (lower rows) their anomalies relative to the 1986–2021 means for different phases of the decadal variability. All data are detrended.

Gyre. Southward near-surface winds over the Bering Strait also reduced the influx of Pacific water into the Arctic (Figure 8).

During the negative AAF phases (1986–1997 and most recently 2011–2021), suppressed BH and AL resulted in anomalous (relative to the 1986–2021 means) anticyclonic winds over the Gulf of Alaska and the eastern Bering Sea, while cyclonic winds were prevalent over the central Arctic (Figure 7). The reduction in the SLP gradient coincided with anomalously low SATs in the Canada Basin over the 2011–2021 decade, while the eastern Bering Sea shelf exhibited warm anomalies. Anomalous winds drove ice convergence in the southern Beaufort Gyre and ice divergence over the Siberian and northern Bering Sea shelves. Northward winds boosted the influx of Pacific water through Bering Strait into the Chukchi Sea (Figure 8).

3.4 | Orientation of SLP Gradients

The AAF index provides a measure of AL and BH co-variability and helps document and discern the role of SLP gradients in shaping the regional geostrophic wind regimes either connecting (if meridional) or inhibiting (if zonal) sub-Arctic and Arctic interactions across the PAR region. Therefore, identifying the orientation—zonal versus meridional—of the BH-AL SLP gradients is crucial to understanding how the PAR responds to climate forcing. We define the orientation of the SLP gradients by angle α referenced to East = 0° and increasing counterclockwise such that $\alpha = 90°$ indicates a south-to-north SLP gradient that is associated with a pure zonal westward geostrophic wind. Thus, $\alpha < 90°$ denotes conditions in which geostrophic winds across the PAR tend to have a northward component and $\alpha > 90°$ is associated with southward winds.

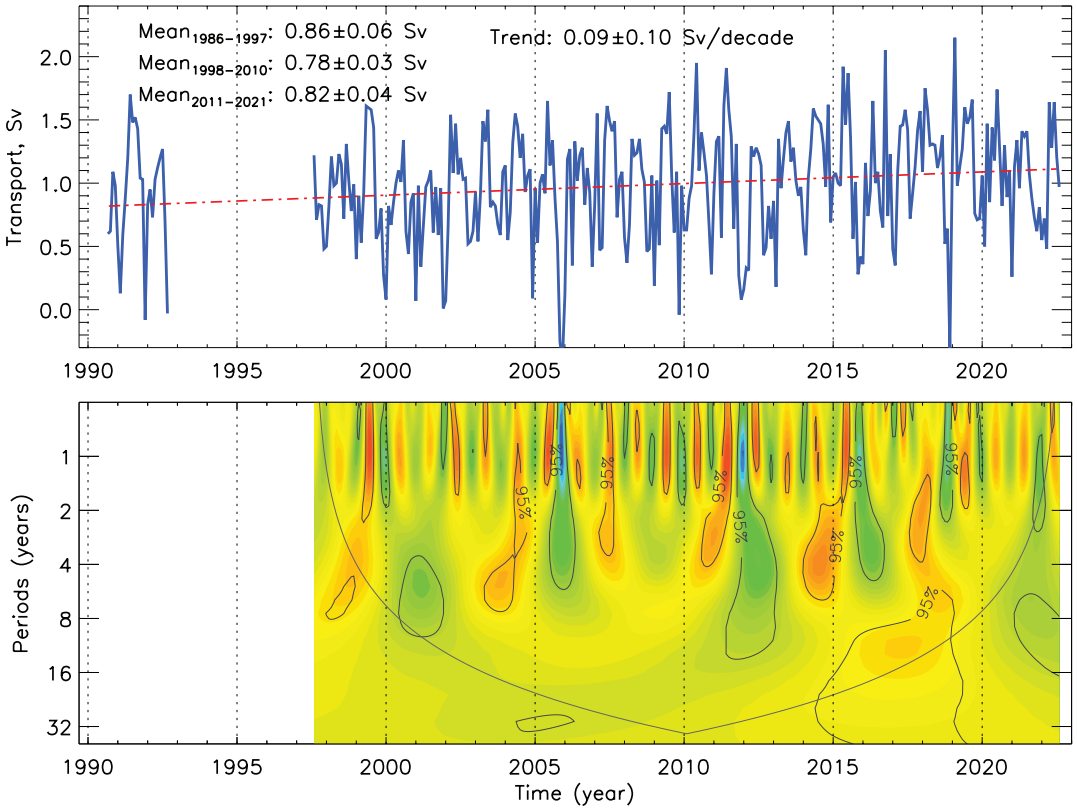

FIGURE 8 | Time series (top) and its wavelet (bottom) of monthly water transport through the Bering Strait from mooring observations (Woodgate and Peralta-Ferriz 2021). Means for 1986–1997, 1998–2010 and 2011–2021 are based on detrended time series.

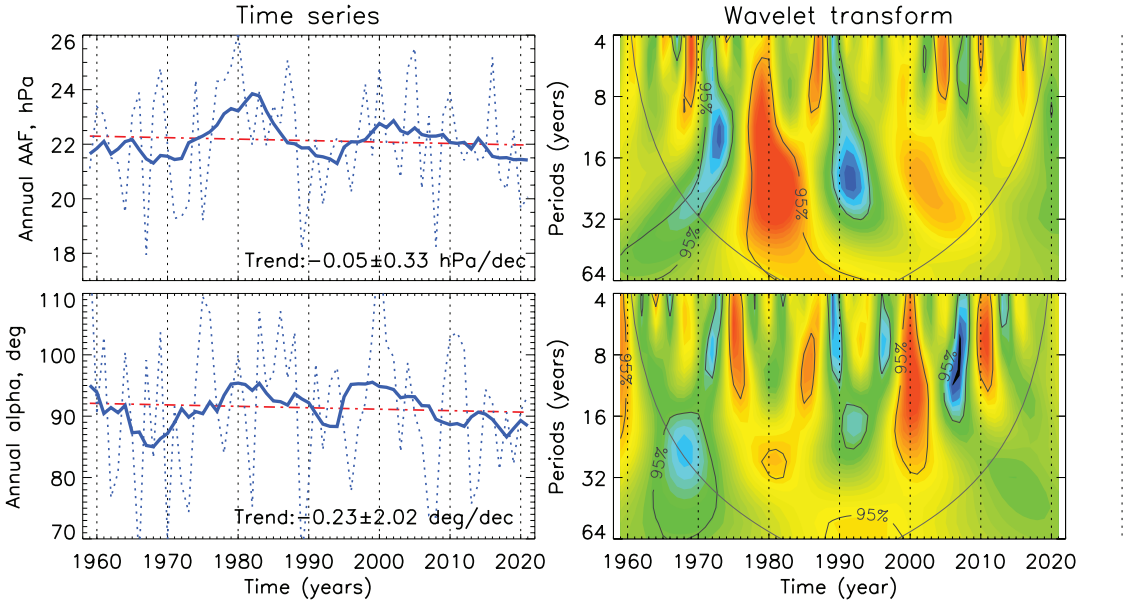

FIGURE 9 | Time series (left) and their wavelets (right) of the AAF index (top) and the BG-AL SLP gradient angle α, or slope (bottom). The α (the angle created by the line segment between the blue and red dots in Figure 2, top) is expressed as an angle from the east in a counterclockwise orientation (degrees). $\alpha = 90°$ denotes a geostrophic wind that is solely zonal and blows westward, whereas a slope of larger (lesser) angle denotes the presence of a southward (northward) geostrophic wind component. Note that the AAF and α time series are correlated at $R = 0.68$ ($p < 0.001$).

The time series of α is shown and compared with the annual AAF time series in Figure 9, which shows that the BH-AL SLP gradients are predominantly south–north oriented (mean $\alpha = 91.3°$) and the regional zonal geostrophic winds are prevailing. There is some interannual variability in the system (the standard deviation of $\alpha = 11.9°$). However, as with the AAF, there

is strong decadal variability, which is in phase with the AAF decadal phases, as corroborated by the correlation between the 10-year running mean time series ($R = 0.68$) and wavelet analysis (Figure 9). Thus, positive AAF phases are associated with $\alpha > 90°$, whereas negative AAF phases (including 2011–2021) are dominated by $\alpha < 90°$. We also note that there was no significant temporal change in the distance between the BG and AL centres (not shown). One of many consequences of the preponderance of northward winds over the PAR is the tendency for stronger poleward water mass transport through Bering Strait (Figures 8 and 10).

Figure 10 provides another illustration of how regional patterns in the ocean, sea ice, and atmosphere are shaped by the direction of the BH-AL SLP gradients. We did not attempt to differentiate the effects of decadal and higher frequency interannual variability in this analysis, so all of the α values were grouped into three categories: large, small, and near normal. The cumulative probability distribution function was used to define the categories, with $\alpha = 87.0°$ and 96.7° separating lower-than-normal (small), normal, and higher-than-normal (large) values (Figure 10b). Composite maps of SLP and corresponding geostrophic wind, SAT and SIC for these three categories of α are

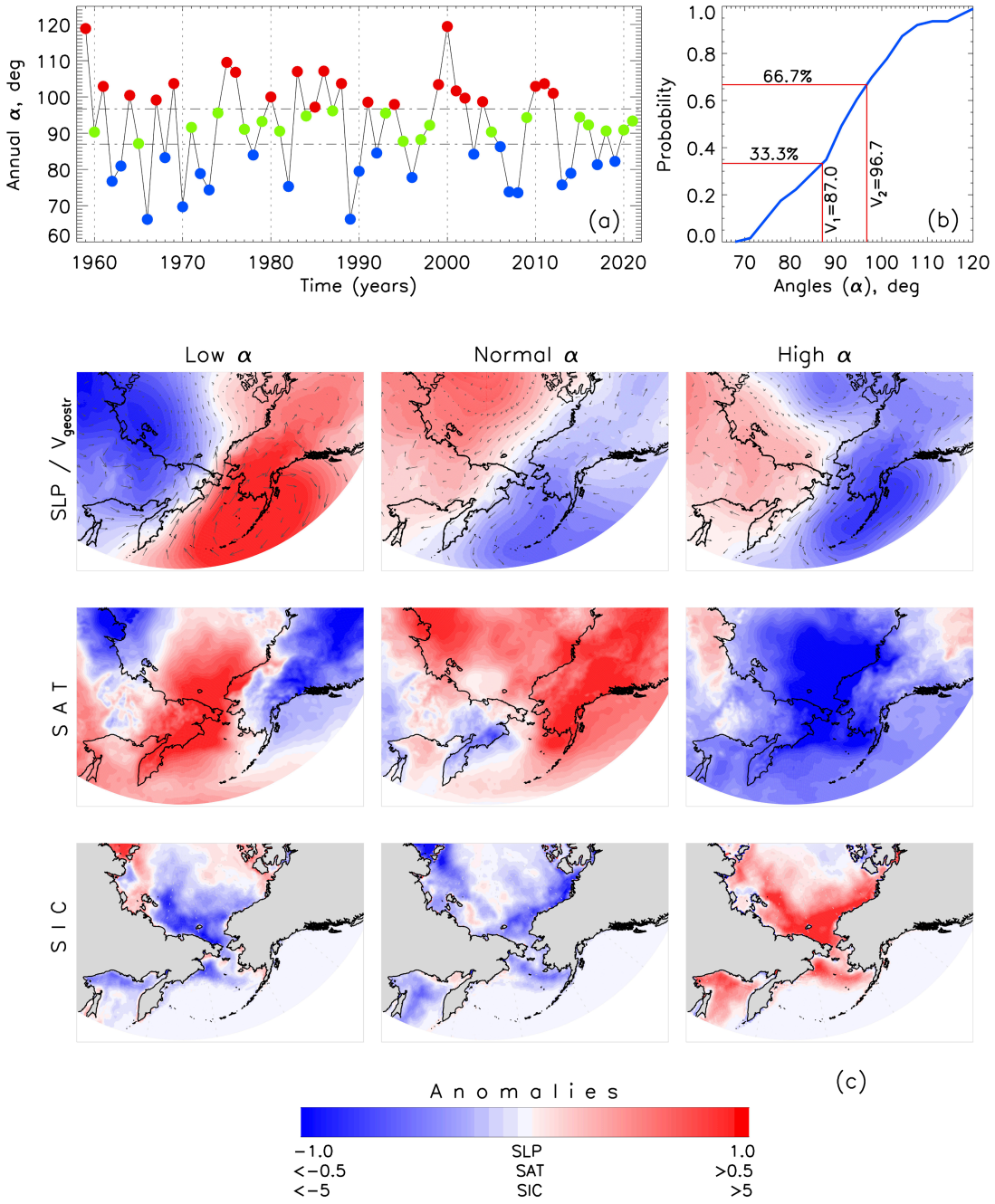

FIGURE 10 | Response of the PAR to orientation of the BG-AL SLP gradient. (a) Time series of the annual BG-AL SLP gradient orientation (angle, α) with red, green, and blue dots indicating higher than normal, normal, and lower than normal categories of α. (b) Cumulative probability distribution of function of α used to define the three categories. (c) Composite maps of SLP and surface geostrophic winds (vectors, V_{geostr}), SAT, and SIC corresponding to lower than normal (small), normal, and higher than normal (large) α.

shown in Figure 10c. It is evident that for small-α years, such as many of the recent 2011–2021 period, the AL is weakened while the SLP is decreased in the Eurasian part of the Arctic. Amplified northward winds bring additional heat and elevated SAT across much of the PAR, reducing sea ice cover. The opposite tendencies apply to the large-α years.

The BH-AL orientation strongly depends on the shift of AL west–east longitude location from the eastern to western Bering Sea (Rodionov, Overland, and Bond 2005). When the AL is in its western location (which corresponds to $\alpha < 90°$), northward winds in the eastern Bering Sea contribute to the weakening of the AAF as in 2018 and 2019. Historically, the western location is less frequent but can occur several times a decade (Overland et al. 2024). Nevertheless, we do see annual and seasonal migration trends superimposed on the spatial variability of the BH (Figure S5) and to a lesser extent the AL (Figure S6). This projects onto the α, increasing in fall and winter (suggesting enhanced southward flowing geostrophic winds) and decreasing in spring and summer (resulting in a larger northward geostrophic winds) (Figure 1). We also noted decadal fluctuations of α connected to the AAF decadal variability. Due to the longitudinal dependence of the AL position, the AAF index is somewhat constrained. Therefore, a given AAF value may have different practical implications based on the exact position of the BH and AL centres as well as time span of analysis. One consequence could be contrasting SLP anomalies in the Bering Sea between different negative phases of decadal variability (e.g., a positive SLP anomaly and weaker AL in eastern Bering Sea during 1986–1997 but a negative SLP anomaly in the western Bering Sea and stronger AL during 2011–2021).

3.5 | Competing Effects of AO and PNA in Shaping Regional Climate Variability

The relative contributions of the Arctic (represented by AO) and Pacific (represented by PNA) forcing to regional PAR climate variability (represented by AAF) were examined using multivariate regression analysis. The AO and PNA indices (Figure 11a) when used as predictors enable a reasonably successful reconstruction of the AAF variability, as demonstrated by the relatively strong correlation $R = 0.72$ between the original and projected AAF (Figure 11b). Furthermore, Figure 11b shows that when the entire 1959–2021 length of the records is used, the two regression coefficients β differ by a mere 12%. This suggests that, on average, the Arctic and Pacific forcing contribute roughly equally to variability in the PAR. However, the picture is different when we consider the relative contributions of AO and PNA to the AAF variability for the different phases of the decadal mode (Figure 11c). Particularly, it is evident that AO dominates the positive phases (e.g., 1998–2010, when AAF was high) while PNA dominates the negative phases (e.g., 2011–2021, when AAF was low). This tendency is statistically significant over the two most recent phases (beginning in 1998), but it is not well resolved before then. During the recent phase when the AAF is low, the Pacific is the dominant driver of variability in the PAR (see also Figure S7 which shows the AAF and climate index running correlations). This finding partially explains the increased influx of anomalous Pacific waters into the Arctic Ocean through the Bering Strait, creating conditions favourable for increased heat and freshwater content in the Beaufort Gyre halocline and expansion of Pacific species into the Arctic interior (this process was called '*Pacification*' in Polyakov et al. 2020).

3.6 | Ecological Implications of Physical Changes in the PAR

PAR physical changes reflected in the AAF variability have numerous current and future ecological implications, and we isolate here select representative marine and terrestrial examples. The two reference fish indices clearly demonstrate a connection to the AAF (marked in Figure 12 as F1 and F2 indices). A positive trend for F1 (0.69 ± 0.19 km per year) and decadal fluctuations driven by pacification-favouring conditions in recent decades contribute to the northward spread of Pacific species in 1982–2021 (Mueter and Litzow 2008; Stevenson and Lauth 2019). Similarly, a positive trend in F2 (0.0039 ± 0.0031, unitless per year, equivalent to ~0.39% increase in CPUE per year) suggests a modest increase (0.39% per year) in fish and invertebrate biomass over the 1982–2021 period and higher biomass during the negative phase of AAF (Figure 12). Although F2 largely reflects fluctuations in the abundance of a single dominant species (walleye pollock), other species are known to similarly fluctuate in concert with changing environmental conditions with some species increasing and others decreasing (Siddon 2021). Reduced sea ice and warmer bottom temperatures on the Bering shelf are the most likely drivers of these shifts in distribution and abundance.

Impacts of AAF variability also project onto terrestrial productivity. An example is shown using the time-integrated Normalized Difference Vegetation Index (TI-NDVI, unitless), a remotely sensed proxy for Arctic vegetation productivity, where a relationship is found with the AAF index (Figure 13). The correlation value ($R = -0.22$) is not high and is statistically significant at the 92% confidence level. Wavelet analysis shows that statistically significant phases of decadal TI-NDVI fluctuations closely resemble those reported by the AAF (Figure 13). The current (2011–2021) positive trend ($+0.53 \pm 0.47\,\text{decade}^{-1}$) in southwestern Alaska, which indicates that the vegetation is 'greening' (gaining biomass and increasing photosynthetic productivity), was mostly shaped by the positive phase (2011–2021) of the TI-NDVI decadal variability (Figure 13). This is in spite of an overall downward tendency of $-0.086 \pm 0.0020\,\text{decade}^{-1}$ over the longer term of 1982–2021. Local spring sea ice conditions prior to the growing season, which are a fingerprint of climatic changes in PAR represented by AAF, are most likely the main driver of these vegetation alterations (Figure 13).

4 | Discussion and Conclusions

A new mobile AAF index associated with the BH-AL SLP gradients (and thus, zonal and meridional geostrophic winds) is introduced to characterise mechanistic controls of the PAR, located at the confluence of the Arctic and North Pacific.

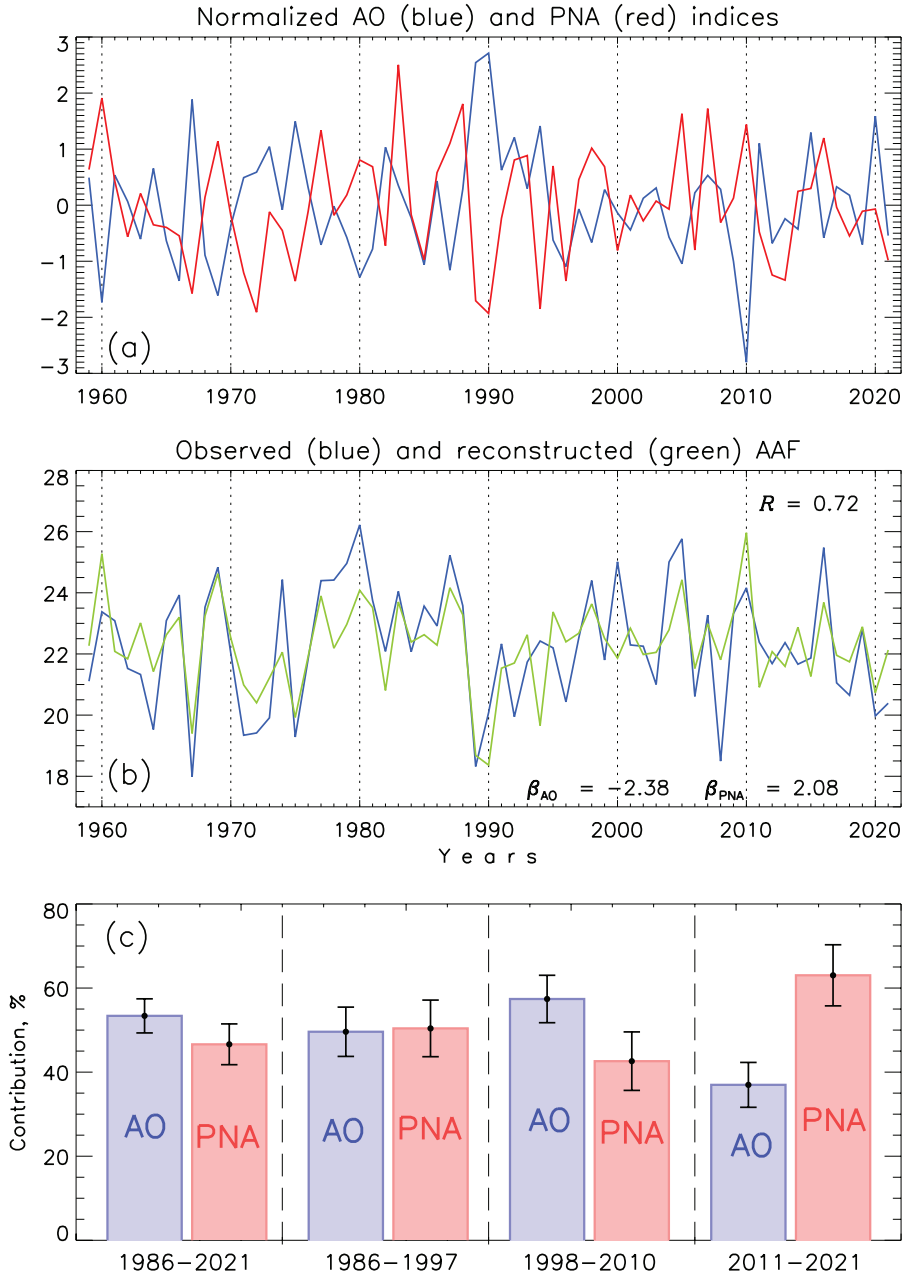

FIGURE 11 | Relative contribution of the AO and PNA to the magnitude of the AAF during the three last phases of the decadal variability. (a) Time series of normalised AO and PNA indices used as predictors in multivariate regression. (b) Original and reconstructed AAF time series using multivariate regression (correlated at $R = 0.72$, $p < 0.001$). (c) The relative contribution of detrended AO and PNA expressed as a percentage (%) to the magnitude of decadal AAF variations.

The BH-AL SLP gradient characterised by the angle between BH and AL is oriented more SW to NE in the most recent period due to the westward displacement of AL explaining the amplified northward component of winds and Pacification. In that, the extratropical Northern Hemisphere modes of the PNA/NPI (north Pacific) and AO (Arctic) have opposing effects that determine the AAF variability, with the decadal time scale emerging as most prominent. PAR variability is dominated by the North Pacific (AL) during low (negative) AAF phase of 2011–2021, while the Arctic (BH) forcing tends to be enhanced during high (positive) AAF phase of 1998–2010. Currently (2011–2021), AAF is low, and the North Pacific is the dominant driver of climatic changes in the PAR. One manifestation of this is increasingly strong Pacification associated with stronger northward winds and water transport through Bering Strait, with consequences for sea ice state and the upper ocean circulation in the PAR and beyond.

The relation between the AAF and the Bering Strait transport suggests that of the various wind-driven mechanisms that exert control on the Bering Strait throughflow (Danielson et al. 2014), coastal sea-level setup/setdown associated with cross-shore Ekman transport in the Bering Sea appears to dominate, even over decadal time scales. For example, Bering Strait transport observed across the last two to three decades (Woodgate 2018) is dominated by upward trend, with a fingerprint of the AAF phasing and associated coastal Siberian shelf

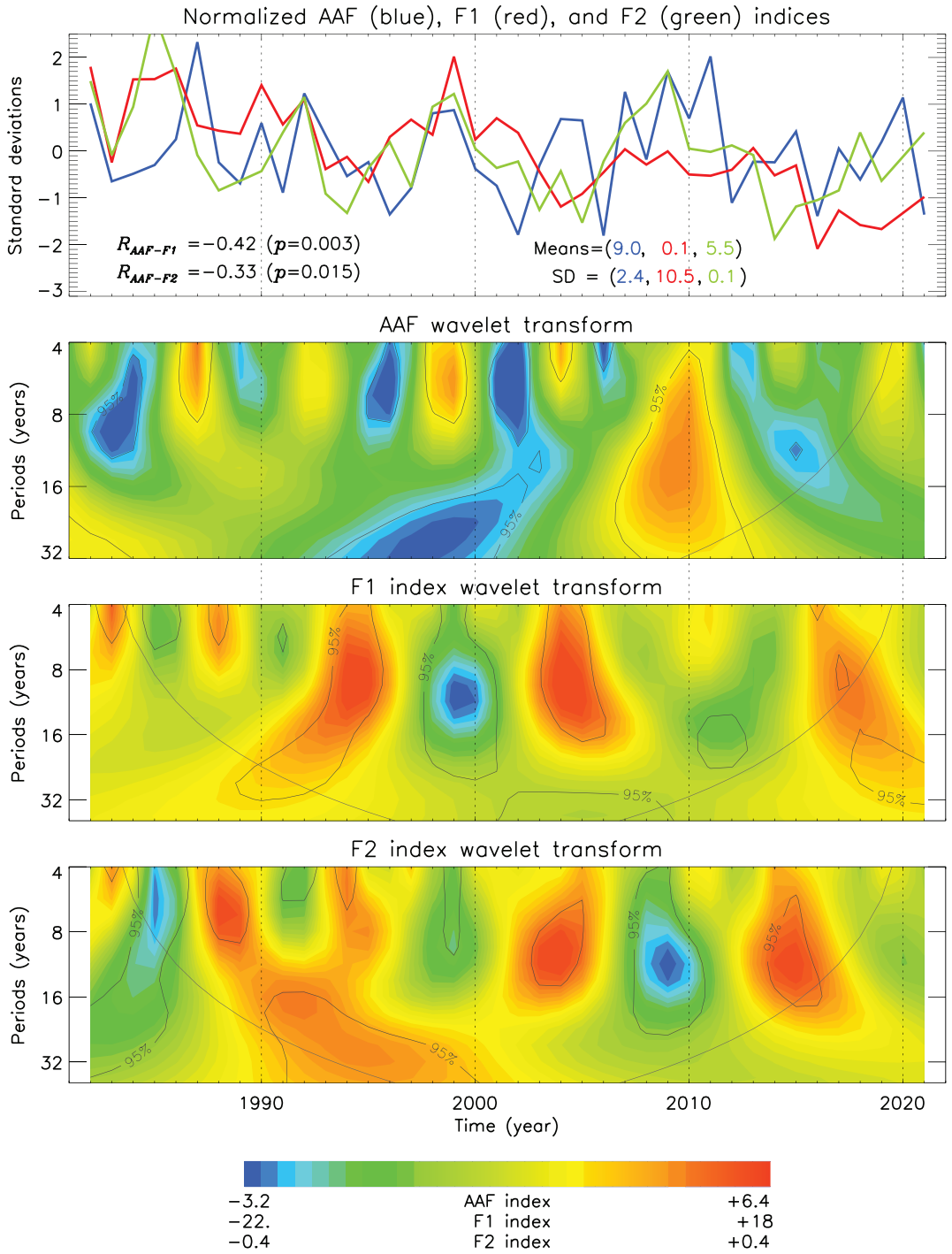

FIGURE 12 | (Top) Time series of normalised (reduced to anomalies by subtracting means and divided by standard deviations, SD) summer AAF (blue, hPa), F1 (red, reflecting north–south displacement of fish on the Bering Sea shelf, km/year) and F2 (green, reflecting the total biomass of major fish and invertebrates on the shelf, kg/ha) indices (the latter two time series are multiplied by minus one). The correlations R between unsmoothed AAF and F1 and F2 indices are modest but statistically significant ($p < 0.05$) at 95% confidence level. (Bottom three panels) Wavelet transforms of the AAF, F1, and F2 indices time series. Note coherent relationship at decadal (e.g., ~20 years) periods.

wind anomalies. In addition to forcing by the AL over the Bering shelf, wind forcing (Danielson et al. 2014; Danielson, Hennon et al. 2020) and fresh water (Peralta-Ferriz and Woodgate 2017) along the north-facing Siberian coastline also impact the Bering Strait flow and fall under the influence of the AAF.

While extratropical teleconnections relate to the variability of the BH, AL, and thus the AAF (e.g., Rodionov, Bond, and Overland 2007; Serreze and Barrett 2011), the possibility of a more remote driver for climatic changes in the PAR should not be ruled out by this approach, however. For example, a strong El Niño typically brings to Alaska warmer autumns and winters

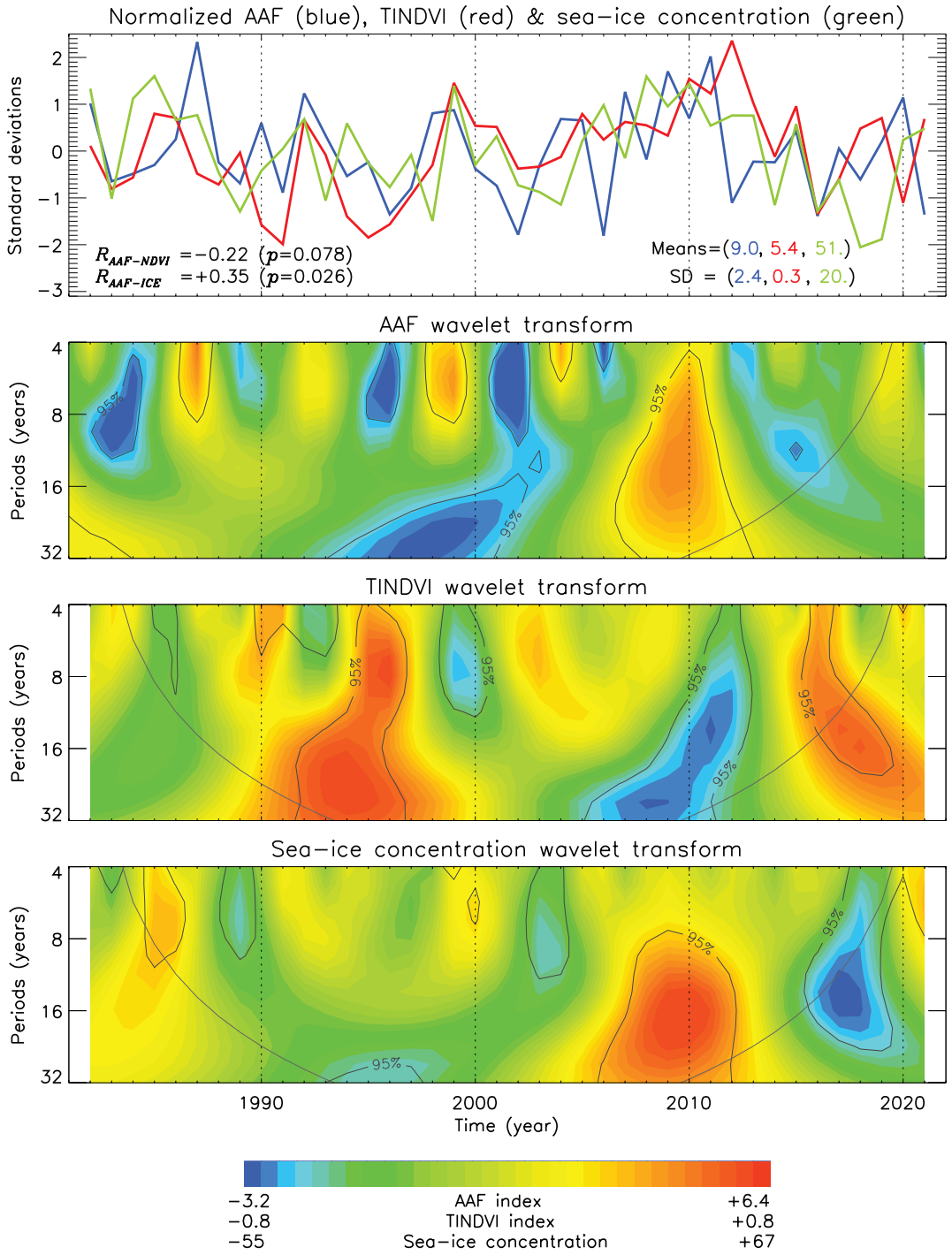

FIGURE 13 | (Top) Time series of normalised (reduced to anomalies by subtracting means and divided by standard deviations) summer AAF (blue, in hPa), TI-NDVI (red, unitless) indices (the latter time series is multiplied by minus one), and regional (eastern Bering Sea 100 km coastal zone) sea ice concentration (green, in %). Means, standard deviations (SD), and correlations (R) based on unsmoothed data with p values are displayed; a statistically significant estimate at a 95% confidence level is indicated by $p < 0.05$. (Bottom three panels) Wavelet transforms of the AAF, TI-NDVI, and sea ice concentration time series. Note coherent relationship at decadal (e.g., ~20 years) periods.

along with more stormy weather as a result of an intensified AL, particularly in the Gulf of Alaska (e.g., Rodionov, Overland, and Bond 2005). The modest (yet statistically significant at 95% confidence level) correlation $R = 0.27$ between the AAF and Niño4 climatic indices indicates that changes in the PAR climate may be influenced by distant, in particular tropical, regions. Tropical–extratropical feedbacks are associated with deterministic linkages across the ocean–atmosphere system, although internal stochastic variability also plays a key role in system state (Di Lorenzo et al. 2013). Deterministic forcings include meridional modes of variability within both the ocean (e.g., Taguchi et al. 2007) and the atmosphere (Alexander et al. 2002). El Niño triggers such teleconnections, affecting both the strength and location of the AL (Trenberth and Hurrell 1994).

In summary, we note that the climate variability of the PAR where the impacts of the Pacific and the Arctic collide and compete, is strong, complex, and distinct from other Arctic regions. Strong decadal variability is prominent, and it is not yet clear if the most recent phase—which was dominated by the Pacification—will change into a new one or return to its previous state. If sea ice cover and associated ocean–atmosphere heat fluxes remain important controls over the atmosphere, then the recent AAF state may persist. Atmospheric circulation across the Arctic and northern North Pacific regions is likely to continue to show considerable variability in the coming decades, both interannually and decadally, with important implications for the physical, geochemical, and ecological components of the PAR earth system.

Author Contributions

Igor V. Polyakov: conceptualization, methodology, software, data curation, formal analysis, validation, investigation, visualization, writing – original draft, writing – review and editing. **Thomas J. Ballinger:** conceptualization, methodology, investigation, formal analysis, supervision, funding acquisition, project administration, writing – original draft, writing – review and editing. **James E. Overland:** writing – original draft, investigation. **Stephen J. Vavrus:** investigation, writing – original draft. **Seth L. Danielson:** investigation, writing – original draft. **Rick Lader:** investigation, writing – original draft. **Uma S. Bhatt:** investigation, writing – original draft, validation. **Amy S. Hendricks:** investigation, writing – original draft, formal analysis, visualization. **Franz J. Mueter:** investigation, writing – original draft, visualization, formal analysis.

Acknowledgements

I.V.P. and T.J.B. acknowledge funding from Office of Naval Research Grant N00014-21-1-2577. I.V.P. was also supported by NSF grant #1724523. S.L.D. was supported by NSF grant #2053084. J.E.O. is supported by the Arctic Research Program of NOAA/GOMO. PMEL contribution number #5612. U.S.B. was supported by NASA's Arctic Boreal Vulnerability Experiment initiative under grant 80NSSC22K1257. SJV was supported by NSF grant #2043727.

Conflicts of Interest

The authors declare no conflicts of interest.

Data Availability Statement

The ERA5 reanalysis data is available from https://cds.climate.copernicus.eu/cdsapp#!/home. Climate indices of monthly atmospheric and ocean time series are obtained from NOAA PSL at https://psl.noaa.gov/data/climateindices/list/. AD index is available from lead author by request and will be archived upon acceptance of the manuscript.

References

Alexander, M. A., I. Blade, M. Newman, J. R. Lanzante, N.-C. Lau, and J. D. Scott. 2002. "The Atmospheric Bridge: The Influence of ENSO Teleconnections on Air–Sea Interaction over the Global Oceans." *Journal of Climate* 15: 2205–2231.

Baker, M. R., E. V. Farley, S. L. Danielson, C. Mordy, K. M. Stafford, and D. M. S. Dickson. 2023. "Integrated Research in the Arctic—Ecosystem Linkages and Shifts in the Northern Bering Sea and Eastern and Western Chukchi Sea." *Deep Sea Research Part II: Topical Studies in Oceanography* 208: 105251. https://doi.org/10.1016/j.dsr2.2023.105251.

Ballinger, T. J., U. S. Bhatt, P. A. Bieniek, et al. 2023. "Alaska Terrestrial and Marine Climate Trends, 1957-2021." *Journal of Climate* 36: 4375–4391. https://doi.org/10.1175/JCLI-D-22-0434.1.

Ballinger, T. J., and J. E. Overland. 2022. "The Alaskan Arctic Regime Shift Since 2017: A Harbinger of Years to Come?" *Polar Science* 32: 100841. https://doi.org/10.1016/j.polar.2022.100841.

Ballinger, T. J., and J. C. Rogers. 2014. "Climatic and Atmospheric Teleconnection Indices and Western Arctic Sea Ice Variability." *Physical Geography* 35: 459–477. https://doi.org/10.1080/02723646.2014.949338.

Ballinger, T. J., J. E. Walsh, U. S. Bhatt, et al. 2021. "Unusual West Arctic Storm Activity During Winter 2020: Another Collapse of the Beaufort High?" *Geophysical Research Letters* 48: e2021GL092518. https://doi.org/10.1029/2021GL092518.

Bhatt, U. S., D. A. Walker, M. K. Raynolds, et al. 2021. "Climate Drivers of Arctic Tundra Variability and Change Using an Indicators Framework." *Environmental Research Letters* 16: 055019. https://doi.org/10.1088/1748-9326/abe676.

Box, J. E., W. T. Colgan, T. R. Christensen, et al. 2019. "Key Indicators of Arctic Climate Change: 1971-2017." *Environmental Research Letters* 14: 045010. https://doi.org/10.1088/1748-9326/aafc1b.

Brooks, C. E. P., and N. Carruthers. 1953. *Handbooks of Statistical Methods in Meteorology*. London, UK: Meteorological Office.

Comiso, J. C., and F. Nishio. 2008. "Trends in the Sea Ice Cover Using Enhanced and Compatible AMSR-E, SSM/I, and SMMR Data." *Journal of Geophysical Research* 113: C02S07.

Cox, C. J., R. S. Stone, D. C. Douglas, D. M. Stanitski, and M. R. Gallagher. 2019. "The Aleutian Low-Beaufort Sea Anticyclone: A Climate Index Correlated With the Timing of Springtime Melt in the Pacific Arctic Cryosphere." *Geophysical Research Letters* 46: 7464–7473. https://doi.org/10.1029/2019GL083306.

Crawford, A. D., J. V. Lukovich, M. R. McCrystall, J. C. Stroeve, and D. G. Barber. 2022. "Reduced Sea Ice Enhances Intensification of Winter Storms Over the Arctic Ocean." *Journal of Climate* 35: 3353–3370. https://doi.org/10.1175/JCLI-D-21-0747.1.

Danielson, S. L., O. Ahkinga, C. Ashjian, et al. 2020. "Manifestation and Consequences of Warming and Altered Heat Fluxes Over the Bering and Chukchi Seas Continental Shelves." *Deep-Sea Research Part II: Topical Studies in Oceanography* 177: 104781. https://doi.org/10.1016/j.dsr2.2020.104781.

Danielson, S. L., T. D. Hennon, K. S. Hedstrom, et al. 2020. "Oceanic Routing of Wind-Sourced Energy along the Arctic Continental Shelves." *Frontiers in Marine Science* 7: 509.

Danielson, S. L., T. J. Weingartner, K. S. Hedstrom, et al. 2014. "Coupled Wind-Forced Controls of the Bering–Chukchi Shelf Circulation and the Bering Strait Throughflow: Ekman Transport, Continental Shelf Waves, and Variations of the Pacific–Arctic Sea Surface Height Gradient." *Progress in Oceanography* 125: 40–61.

Di Lorenzo, E., V. Combes, J. E. Keister, et al. 2013. "Synthesis of Pacific Ocean Climate and Ecosystem Dynamics." *Oceanography* 26, no. 4: 68–81.

Duffy, P. A., J. E. Walsh, J. M. Graham, D. H. Mann, and T. S. Rupp. 2005. "Impacts of Large-Scale Atmospheric-Ocean on Alaskan Fire Season Severity." *Ecological Applications* 15: 1317–1330.

Ershova, E. A., R. R. Hopcroft, K. N. Kosobokova, et al. 2015. "Long-Term Changes in Summer Zooplankton Communities of the Western Chukchi Sea, 1945–2012." *Oceanography* 28, no. 3: 100–115.

Franzke, C., and S. B. Feldstein. 2005. "The Continuum and Dynamics of Northern Hemisphere Teleconnection Patterns." *Journal of the Atmospheric Sciences* 62: 3250–3267.

Frey, K. E., G. W. K. Moore, L. W. Cooper, and J. Grebmeier. 2015. "Divergent Patterns of Recent Sea Ice Cover Across the Bering,

Chukchi, and Beaufort Seas of the Pacific Arctic Region." *Progress in Oceanography* 136: 32–49. https://doi.org/10.1016/j.pocean.2015.05.009.

Frost, G. V., U. S. Bhatt, M. J. Macander, A. S. Hendricks, and M. T. Jorgenson. 2021. "Is Alaska's Yukon–Kuskokwim Delta Greening or Browning? Resolving Mixed Signals of Tundra Vegetation Dynamics and Drivers in the Maritime Arctic." *Earth Interactions* 25, no. 1: 76–93.

Grant, A. N., S. Brönnimann, T. Ewen, and A. Nagurny. 2009. "A New Look at Radiosonde Data Prior to 1958." *Journal of Climate* 22: 3232–3247. https://doi.org/10.1175/2008JCLI2539.1.

Hauser, D. D. W., A. V. Whiting, A. R. Mahoney, et al. 2021. "Co-Production of Knowledge Reveals Loss of Indigenous Hunting Opportunities in the Face of Accelerating Arctic Climate Change." *Environmental Research Letters* 16: 095003. https://doi.org/10.1088/1748-9326/ac1a36.

Hendricks, A., U. Bhatt, G. Frost, et al. 2023. "Decadal Variability in Spring Sea Ice Concentration Linked to Summer Temperature and NDVI on the Yukon–Kuskokwim Delta." *Earth Interactions* 27, no. 1.

Hersbach, H., B. Bell, P. Berrisford, et al. 2020. "The ERA5 Global Reanalysis." *Quarterly Journal of the Royal Meteorological Society* 146: 1999–2049. https://doi.org/10.1002/qj.3803.

Huang, B., C. Liu, V. Banzon, et al. 2021. "Improvements of the Daily Optimum Interpolation Sea Surface Temperature (DOISST) Version 2.1." *Journal of Climate* 34: 2923–2939. https://doi.org/10.1175/JCLI-D-20-0166.1.

Huntington, H. P., S. L. Danielson, F. K. Wiese, et al. 2020. "Evidence Suggests Potential Transformation of the Pacific Arctic Ecosystem is Underway." *Nature Climate Change* 10: 342–348. https://doi.org/10.1038/s41558-020-0695-2.

Mallett, R. D. C., J. C. Stroeve, S. B. Cornish, et al. 2021. "Record Winter Winds in 2020/21 Drove Exceptional Arctic Sea Ice Transport." *Communications Earth & Environment* 2: 149. https://doi.org/10.1038/s43247-021-00221-8.

McAfee, S. A. 2014. "Consistency and the Lack Thereof in Pacific Decadal Oscillation Impacts on North American Winter Climate." *Journal of Climate* 27, no. 19: 7410–7431. https://doi.org/10.1175/JCLI-D-14-00143.1.

McAfee, S. A. 2016. "Uncertainty in Pacific Decadal Oscillation Indices Does Not Contribute to Teleconnection Instability." *International Journal of Climatology* 37, no. 8: 3509–3516. https://doi.org/10.1002/joc.4918.

Moore, G. W. K., I. A. Renfrew, and R. S. Pickart. 2013. "Multidecadal Mobility of the North Atlantic Oscillation." *Journal of Climate* 26: 2453–2466. https://doi.org/10.1175/JCLI-D-12-00023.1.

Moore, G. W. K., A. Schweiger, J. Zhang, and M. Steele. 2018. "Collapse of the 2017 Winter Beaufort High: A Response to Thinning Sea Ice?" *Geophysical Research Letters* 45: 2860–2869. https://doi.org/10.1002/2017GL076446.

Mueter, F. J., and M. A. Litzow. 2008. "Sea Ice Retreat Alters the Biogeography of the Bering Sea Continental Shelf." *Ecological Applications* 18: 309–320.

Nowacki, G., P. Siddon, M. Fleming, T. Brock, and M. T. Jorgenson. 2003. "Ecoregions of Alaska: 2001." USGS Open-File Rep. 2002-29. https://doi.org/10.3133/ofr2002297.

Overland, J. E., J. A. Francis, E. Hanna, and M. Wang. 2012. "The Recent Shift in Early Summer Arctic Atmospheric Circulation." *Geophysical Research Letters* 39: L19804. https://doi.org/10.1029/2012GL053268.

Overland, J. E., E. Siddon, G. Sheffield, T. J. Ballinger, and C. Szuwalski. 2024. "Transformative Ecological and Human Impacts From Diminished Sea Ice in the Northern Bering Sea." *Weather, Climate, and Society* 16: 303–313. https://doi.org/10.1175/WCAS-D-23-0029.1.

Overland, J., E. Spencer, G. Sheffield, T. Ballinger, and C. Szuwalski. 2024. "Transformative Ecological and Human Impacts from Climate Change and Diminished Sea Ice in the Northern Bering Sea." *Weather, Climate, and Society* 16, no. 2: 303–313. https://doi.org/10.1175/WCAS-D-23-0029.1.

Overland, J. E., and M. Wang. 2005. "The Third Arctic Climate Pattern: 1930s and Early 2000s." *Geophysical Research Letters* 32, no. 23: L23808. https://doi.org/10.1029/2005GL024254.

Overland, J. E., M. Wang, and T. J. Ballinger. 2018. "Recent Increased Warming of the Alaskan Marine Arctic Due to Midlatitude Linkages." *Advances in Atmospheric Sciences* 35: 75–84. https://doi.org/10.1007/s00376-017-7026-1.

Panofsky, H. A., and G. W. Brier. 1958. *Some Applications of Statistics to Meteorology*. University Park, PA: Mineral Industries Extension Services, College of Mineral Industries, Pennsylvania State University.

Papineau, J. M. 2001. "Wintertime Temperature Anomalies in Alaska Correlated With ENSO and PDO." *International Journal of Climatology* 21: 1577–1592. https://doi.org/10.1002/joc.686.

Peralta-Ferriz, C., and R. A. Woodgate. 2017. "The Dominant Role of the East Siberian Sea in Driving the Oceanic Flow Through the Bering Strait—Conclusions from GRACE Ocean Mass Satellite Data and in Situ Mooring Observations Between 2002 and 2016." *Geophysical Research Letters* 44, no. 22: 11–472.

Pinzon, J., and C. Tucker. 2014. "A Non-stationary 1981–2012 AVHRR NDVI3g Time Series." *Remote Sensing* 6: 6929–6960.

Pinzon, J. E., E. W. Pak, C. J. Tucker, U. S. Bhatt, G. V. Frost, and M. J. Macander. 2023. *Global Vegetation Greenness (NDVI) From AVHRR GIMMS-3G+, 1981-2022*. Oak Ridge, TN: ORNL DAAC. https://doi.org/10.3334/ORNLDAAC/2187.

Polyakov, I. V., M. B. Alkire, B. A. Bluhm, et al. 2020. "Borealization of the Arctic Ocean in Response to Anomalous Advection From Sub-Arctic Seas." *Frontiers in Marine Science* 7: 491. https://doi.org/10.3389/fmars.2020.00491.

Polyakov, I. V., R. B. Ingvaldsen, A. V. Pnyushkov, et al. 2023. "Fluctuating Atlantic Inflows Modulate Arctic Atlantification." *Science* 381: 972–979. https://doi.org/10.1126/science.adh5158.

Portis, D. H., J. E. Walsh, M. El Hamly, and P. J. Lamb. 2001. "Seasonality of the North Atlantic Oscillation." *Journal of Climate* 14, no. 9: 2069–2078. https://doi.org/10.1175/1520-0442(2001)014<2069:SOTNAO>2.0.CO;2.

Proshutinsky, A., D. Dukhovskoy, M. L. Timmermans, R. Krishfield, and J. L. Bamber. 2015. "Arctic Circulation Regimes." *Philosophical Transactions of the Royal Society A: Mathematical, Physical and Engineering Sciences* 373, no. 2052: 20140160. https://doi.org/10.1098/rsta.2014.0160.

Rodionov, S. N., N. A. Bond, and J. E. Overland. 2007. "The Aleutian Low, Storm Tracks, and Winter Climate Variability in the Bering Sea." *Deep Sea Research Part II: Topical Studies in Oceanography* 54: 2560–2577. https://doi.org/10.1016/j.dsr2.2007.08.002.

Rodionov, S. N., J. E. Overland, and N. A. Bond. 2005. "The Aleutian Low and Winter Climatic Conditions in the Bering Sea. Part I: Classification." *Journal of Climate* 18, no. 1: 16–177. https://doi.org/10.1175/JCLI3253.1.

Serreze, M. C., and A. P. Barrett. 2011. "Characteristics of the Beaufort Sea High." *Journal of Climate* 24: 159–182. https://doi.org/10.1175/2010JCLI3636.1.

Serreze, M. C., A. H. Lynch, and M. P. Clark. 2001. "The Arctic Frontal Zone as Seen in the NCEP-NCAR Reanalysis." *Journal of Climate* 14: 1550–1567.

Siddon, E. 2021. *Ecosystem Status Report 2021: Eastern Bering Sea, Stock Assessment and Fishery Evaluation Report*. Anchorage, AL: North Pacific Fishery Management Council.

Stabeno, P. J., and S. W. Bell. 2019. "Extreme Conditions in the Bering Sea (2017-2018): Record-Breaking Low Sea Ice Extent." *Geophysical Research Letters* 46: 8952–8959. https://doi.org/10.1029/2019GL083816.

Steele, M., J. Morison, W. Ermold, I. Rigor, M. Ortmeyer, and K. Shimada. 2004. "Circulation of Summer Pacific Halocline Water in the Arctic Ocean." *Journal of Geophysical Research* 109: C02027. https://doi.org/10.1029/2003JC002009.

Stevenson, D. E., and R. R. Lauth. 2019. "Bottom Trawl Surveys in the Northern Bering Sea Indicate Recent Shifts in the Distribution of Marine Species." *Polar Biology* 42, no. 2: 407–421. https://doi.org/10.1007/s00300-018-2431-1.

Szuwalski, C. S., K. Aydin, E. J. Fedewa, B. Garber-Yonts, and M. A. Litzow. 2023. "The Collapse of Eastern Bering Sea Snow Crab." *Science* 382: 6668. https://doi.org/10.1126/science.adf6035.

Tachibana, Y., K. K. Komatsu, V. A. Alexeev, L. Cai, and Y. Ando. 2019. "Warm Hole in Pacific Arctic Sea Ice Cover Forced Mid-Latitude Northern Hemisphere Cooling During Winter 2017-2018." *Scientific Reports* 9: 5567. https://doi.org/10.1038/s41598-019-41682-4.

Taguchi, B., S. P. Xie, N. Schneider, et al. 2007. "Decadal Variability of the Kuroshio Extension: Observations and an Eddy-Resolving Model Hindcast." *Journal of Climate* 20, no. 11: 2357–2377.

Jr. Thoman, R. L., U. S. Bhatt, P. A. Bieniek, et al. 2020. "The Record Low Bering Sea Ice Extent in 2018: Context, Impacts, and an Assessment of the Role of Anthropogenic Climate Change." *BAMS* 101, no. 1: 553–557. https://doi.org/10.1175/BAMS-D-19-0175.1.

Timmermans, M.-L., and J. M. O'Toole. 2023. "The Arctic Ocean's Beaufort Gyre." *Annual Review of Marine Science* 15: 6.1–6.26. https://doi.org/10.1146/annurev-marine-032122-012034.

Timmermans, M. L., A. Proshutinsky, E. Golubeva, et al. 2014. "Mechanisms of Pacific Summer Water Variability in the Arctic's Central Canada Basin." *Journal of Geophysical Research: Oceans* 119, no. 11: 7523–7548.

Timmermans, M.-L., J. Toole, and R. Krishfield. 2018. "Warming of the Interior Arctic Ocean Linked to Sea Ice Losses at the Basin Margins." *Science Advances* 4, no. 8. https://doi.org/10.1126/sciadv.aat6773.

Torrence, C., and G. P. Compo. 1998. "A Practical Guide to Wavelet Analysis." *Bulletin of the American Meteorological Society* 79: 61–78.

Trenberth, K. E., and J. W. Hurrell. 1994. "Decadal Atmosphere-Ocean Variations in the Pacific." *Climate Dynamics* 9: 303–319. https://doi.org/10.1007/BF00204745.

Walsh, J. E., D. H. Bromwich, J. E. Overland, M. C. Serreze, and K. R. Wood. 2018. *100 Years of Progress in Polar Meteorology. A Century of Progress in Atmospheric and Related Sciences: Celebrating the American Meteorological Society Centennial, Meteor. Monogr., No. 59*. Boston: American Meteorological Society. https://doi.org/10.1175/AMSMONOGRAPHS-D-18-0003.1.

Wang, M., Q. Yang, J. E. Overland, and P. Stabeno. 2018. "Sea Ice Cover Timing in the Pacific Arctic: The Present and Projections to Mid-Century by Selected CMIP5 Models." *Deep-Sea Research Part II: Topical Studies in Oceanography* 152: 22–34. https://doi.org/10.1016/j.dsr2.2017.11.017.

Wang, W., C. Jing, and X. Guo. 2024. "Is Only the Wind Field Controlling the Maximum Sea Ice Area in the Bering Sea?" *Journal of Geophysical Research: Oceans* 129: e2023JC020790. https://doi.org/10.1029/2023JC020790.

Woodgate, R. A. 2018. "Increases in the Pacific Inflow to the Arctic From 1990 to 2015, and Insights into Seasonal Trends and Driving Mechanisms From Year-Round Bering Strait Mooring Data." *Progress in Oceanogr* 160: 124–154. https://doi.org/10.1016/j.pocean.2017.12.007.

Woodgate, R. A., and C. Peralta-Ferriz. 2021. "Warming and Freshening of the Pacific Inflow to the Arctic From 1990-2019 Implying Dramatic Shoaling in Pacific Winter Water Ventilation of the Arctic Water Column." *Geophysical Research Letters* 48: e2021GL092528. https://doi.org/10.1029/2021GL092528.

Supporting Information

Additional supporting information can be found online in the Supporting Information section.